

Journal of Materials Chemistry B

Accepted Manuscript



This is an *Accepted Manuscript*, which has been through the Royal Society of Chemistry peer review process and has been accepted for publication.

Accepted Manuscripts are published online shortly after acceptance, before technical editing, formatting and proof reading. Using this free service, authors can make their results available to the community, in citable form, before we publish the edited article. We will replace this *Accepted Manuscript* with the edited and formatted *Advance Article* as soon as it is available.

You can find more information about *Accepted Manuscripts* in the [Information for Authors](#).

Please note that technical editing may introduce minor changes to the text and/or graphics, which may alter content. The journal's standard [Terms & Conditions](#) and the [Ethical guidelines](#) still apply. In no event shall the Royal Society of Chemistry be held responsible for any errors or omissions in this *Accepted Manuscript* or any consequences arising from the use of any information it contains.

Development and characterization of polyethylene glycol-carbon nanotube hydrogel composite

K. Shah, D. Vasileva, A. Karadaghy, S. Zustiak*

Department of Biomedical Engineering

Saint Louis University

3507 Lindell Blvd

St Louis, MO

*Corresponding author:

Department of Biomedical Engineering

Saint Louis University

3507 Lindell Blvd

St Louis, MO

Email: szustiak@slu.edu

Phone: 314-977-8331

Keywords: conductive hydrogel, polyethylene glycol, neural cells, carbon nanotubes, neural tissue engineering

Abstract

Carbon nanotube (CNT)-hydrogel composites are attractive for a variety of neural tissue engineering and drug delivery applications as well as biosensor coatings, transducers and leads. Both materials contribute unique and beneficial properties to the composites. Hydrogels are an excellent mimic of the extracellular matrix due to their hydrophilicity, viscoelasticity and biocompatibility. CNTs, on the other hand, can impart electroconductivity to otherwise insulating materials, improve mechanical stability and guide neuronal cell behavior as well as elicit axon regeneration. Not surprisingly, there has been a surge in the development of various CNT-hydrogel composites including both natural and synthetic polymers. Here, we describe a CNT-polyethylene glycol (PEG) hydrogel composite where the CNTs are entrapped in the hydrogel phase during gelation. The hydrogel crosslinking reaction is based on Michael-type addition which is ideal for *in situ* cell and protein encapsulation. To adequately disperse the highly hydrophobic CNTs in the aqueous polymer solution, we used sonication and surfactants, where bovine serum albumin was found to be an effective and non-cytotoxic dispersant. We demonstrate that the inclusion of the CNTs impeded the hydrogel crosslinking leading to longer gelation times, higher swelling and porosity, and lower storage modulus above a threshold CNT concentration. As anticipated, composite hydrogel resistivity decreased with the incorporation of CNTs and was dependent on both CNT loading and dispersion. Importantly, unlike the PEG hydrogel alone, the PEG-CNT hydrogel composite was capable of supporting high neural cell viability where the CNTs provided sites for cell attachment.

1. Introduction

Hydrogels, which are highly water-swollen polymer networks, have structural and mechanical similarity to the extracellular matrix (ECM) and an ability to protect the activity of biomolecules, have become an integral part of many tissue engineering and drug delivery applications.¹ Accordingly, a need has arisen to develop hydrogel composites with multimodal functionalities. With the development of better and more affordable techniques to grow carbon nanotubes (CNTs),² with more thorough understanding of their properties^{3,4} and the implications for living systems,⁵⁻⁷ a type of composite materials that are quickly gaining momentum are CNT-hydrogel composites.⁸⁻¹⁰ There are multiple ways in which CNTs are efficacious in enhancing the hydrogels' already excellent properties: improving mechanical stability, imparting electroconductivity, as well as serving as cell or macromolecule attachment sites or drug delivery vehicles, usually, upon functionalization.¹⁰ For example, CNTs embedded in immunoprotective, nanoporous and inert hydrogels such as polyethylene glycol (PEG), where the CNTs impart electroconductivity, are very attractive as thin film coating for neural electrodes and other neural interfaces.^{11,12} Such coatings are being investigated for their ability to prevent cellular encapsulation and scar tissue formation as well as alleviate the mechanical modulus mismatch between the tissue and the electrode, ultimately, improving long-term implantation outcomes.¹³ CNT-hydrogel composites are also explored for a variety of other neural tissue engineering applications due to the complementary properties of both materials: the hydrophilicity, viscoelasticity and biocompatibility of the hydrogels on one hand and the ability of CNTs to impart electroconductivity and guide neuronal cell behavior as well as elicit axon regeneration on the other.¹⁴ Importantly, while concern about CNT biocompatibility remains, it has been demonstrated that toxicity and carcinogenicity of CNTs are greatly reduced when the CNTs are embedded in a hydrogel matrix.⁹

Not surprisingly, various CNT-hydrogel composites have been developed, including both natural and synthetic polymers such as polyacrylamide,¹⁵ polymethacrylic acid,¹⁶ polysaccharides,¹⁷ gelatin,^{18, 19} collagen,^{6, 20} and PEG^{3, 13} among others. We elected to work with a PEG hydrogel due to its hydrophilicity, biocompatibility, inertness, and tight control and tunability of physical, mechanical and biochemical properties.²¹ Furthermore, PEG hydrogels have shown promise as neural and neural stem cell scaffolds^{22, 23} or neural cell delivery vehicles,²⁴ CNT-PEG-acrylate hydrogels have shown excellent promise as neural electrode coatings,^{13, 25} and PEG-functionalized CNTs have been shown to promote neural regeneration.²⁶ Here, we focus on the development and detailed characterization of CNT-PEG hydrogel composite and its ability to support neural cell culture. While some CNT-hydrogel composites based on photopolymerizable PEG-acrylate have been developed,^{3, 13, 25} here we focus on developing a composite where crosslinking is initiated by a Michael-type addition reaction between an acrylate and a thiol functional groups. The benefits of this chemistry, which include a mild crosslinking at physiological conditions compatible with cell and biomolecules encapsulation, have been well described.^{21, 27} Photopolymerizable PEG on the other hand, while successfully used for cell and protein encapsulation,²⁸ could have unforeseen harmful effects on cells or biomolecules due to the UV irradiation or the nature of the photoinitiators used.^{29, 30} Here we describe a hydrogel that consists of a 4-arm PEG-acrylate and a PEG-dithiol crosslinker; however, similar reaction chemistry can be applied to any unsaturated terminal carbon and a thiol moiety, including the cysteine residues of peptides. To the best of our knowledge, this is the first work describing the effect of CNT incorporation on a PEG hydrogel properties including compatibility with cell encapsulation where PEG is crosslinked via a Michael-type addition reaction. The developed

composite hydrogel has many potential applications in neural tissue engineering and drug delivery especially where *in-situ* cell or protein encapsulation is desired.

2. Materials and Methods

2.1. Materials

All reagents were purchased from Sigma Aldrich (St. Louis, MO) and used as is unless otherwise noted. The materials used in this study were obtained as follows: 4-arm polyethylene glycol acrylate (4-arm PEG-Ac, MW 10,000) from Jen Kem (Plano, TX), polyethylene glycol dithiol (PEG-diSH) linear crosslinker (MW 3,400) from Laysan Bio (Arab, AL), silicone spacers from Grace Bio-Labs (Bend, Oregon), glass plates (10 cm x 8.25 cm) from Bio-Rad Laboratories (Hercules, CA), Rain-X from Rain-X (Houston, TX) and Kimwipes from Kimberly-Clark Professional (Roswell, GA). A sample of semiconducting multiwall carbon nanotubes (MWCNTs) (20 ± 3 nm in diameter and 3 ± 2 μ m in length) produced via catalytic chemical vapor deposition was generously provided from MerCorp (Tucson, AZ). Adherent PC12 pheochromocytoma cells were obtained from ATCC (Manassas, VA). RPMI media and 10% fetal bovine serum were purchased from Hyclone Laboratories (GE Healthcare Life Sciences, Logan, UT), 3,3' – dioctadecyloxycarbocyanine perchlorate (DiOC) and propidium iodide (PI) were obtained from Life Technologies (Carlsbad, CA), Sylgard 182 Silicone Elastomer Base and Curing Agent were obtained from Dow Corning Corporation (Midland, MI), and GelBond sheets (124 mm x 258 mm) were purchased from GE Healthcare (Uppsala, Sweden).

2.2. Polyethylene Glycol Hydrogel Preparation

First, 20% w/v stock solution of 4-arm PEGAc was prepared by dissolution in a 0.3 M triethanolamine (TEA) in phosphate buffered saline (PBS, 1X, pH 8) and used immediately or stored for up to 1 week at 4°C. To prepare a hydrogel, 4-arm PEGAc was reacted with PEG-diSH at a 1:1 molar ratio of Ac:SH. PEG-diSH was added as a solid powder immediately prior to gel formation to avoid premature deprotonation of the thiol group. Additional TEA buffer was added to achieve a desired final PEG concentration. Unless specified otherwise, the hydrogel concentration used for this study was 7.5% w/v in PEG (38.8 mM in SH and Ac end groups). The solution was thoroughly mixed by vortexing for 30 sec, pipetted between hydrophobic-coated glass slides separated by 1 mm silicone spacers and allowed to gel for 30 min at room temperature. To prepare hydrophobic-coated glass slides, Rain-X was applied and the slides were allowed to dry at room temperature for 10 min. Residual Rain-X was carefully wiped with a KimWipe.

2.3. Dispersion of CNTs

Dispersion of CNTs in PEG solution was measured as a function of sonication time and surfactant. Briefly, CNTs were added to a 10% w/v linear non-functionalized PEG-diOH, 4-arm PEG-Ac or PEG-diSH solution at a concentration of 0.05% w/v and dispersed within the solution using a probe sonicator (Fisher Scientific, Waltham, MA) operating at a frequency of 6.75 kHz for 10 min. Two dispersion time regimes were tested: 20 sec on and 10 sec off and (20 on/10 off) and 1 sec on and 1 sec off (1 on/1 off). Additionally, various surfactants were added prior to sonication to aid the dispersion: bovine serum albumin (BSA) at 0.05% w/v (for 0.01% - 0.10% w/v CNTs), 0.2% w/v (for 0.2% w/v CNTs) and 1.2% w/v (for 1.2% w/v CNTs), laminin at 10% w/v, dimethyl sulfoxide (DMSO) at 1% w/v, and sodium cholate (SC) at 0.1% and 1.0% w/v.

Upon dispersion, phase contrast images of the solutions were taken at 10X magnification (Zeiss, Axiovert 200M, Oberkochen, Germany). Dispersion was quantified by measuring the average area of the CNT aggregates using ImageJ free software (image processing program developed by the National Institutes of Health). Additionally, better dispersion was correlated to increased absorbance values. Dispersed composite solutions were placed in a quartz cuvette and absorbance (400 – 1000 nm scan) was measured on Spectra MAX Plus spectrophotometer (Molecular Devices, Sunnyvale, CA). Absorbance values of surfactant solutions in the absence of CNTs was taken as a baseline and subtracted from the absorbance readings of the solution in the presence of CNTs. To visualize CNT dispersion within the PEG hydrogels, 1 mm thick composite hydrogels were precisely cross-sectioned with a dissecting blade into 10 μm thin slices and imaged using a confocal microscope (Olympus FV1000 Scanning Confocal microscope, Central Valley, CA, USA) at 5X zoom. CNTs aggregate size as a function of hydrogel depth was analyzed by ImageJ software to also account for settling of CNTs during gelation.

2.4. Gelation Time

To measure gelation time of the hydrogel as a function of CNT concentration, the inverted tube method was used.³¹ Briefly, 50 μl of the hydrogel precursor solution was pipetted into a microfuge tube and inverted at regular time intervals. Gelation time was noted after the occurrence of the sol-gel transition, i.e. when the gel precursor solution stopped flowing.

2.5. Rheological Testing

A rheometer (AR 2000EX, TA Instruments New Castle, DE, USA) was utilized for hydrogel mechanical testing. For rheological analysis, 300 μl hydrogel samples were prepared between two hydrophobic-treated glass plates separated 1 mm apart by silicone spacers. After gelation, the hydrogels were allowed to swell for 24 hrs in distilled (DI) water and cut to 20 mm in diameter with a cookie cutter. Excess moisture was carefully blotted with a KimWipe and the sample was then placed directly under the 20 mm parallel plate upper geometry. The gap between the upper geometry and Peltier plate was lowered until a normal force of 0.20 N was established. The storage modulus, G' , and loss modulus, G'' , were measured at 2% strain for low angular frequency of 1-10 Hz. All measurements were performed at room temperature.

2.6. Hydrogel Swelling and Mesh Size

To test swellability, hydrogels were soaked in DI water for 24 hrs and weighed (XS204 DeltaRange Scale, Mettler Toledo, Columbus, OH) after carefully blotting excess surface water with a KimWipe. The swollen mass, M_s , was recorded. The gels were then allowed to dry at 60°C for 48 hrs and weighed again to record their dry weight, M_d . A mass swelling ratio, Q_M , was determined as:^{21, 32}

$$Q_M = \left(\frac{M_s}{M_d} \right) \quad (1)$$

Q_M was further used to calculate hydrogel mesh size, ζ . The mesh size was determined by a modified Flory-Rehner theory³³ for a neutral hydrogel prepared in water by first calculating the molecular weight between cross links, M_c :

$$\frac{1}{M_c} = \frac{2}{M_n} - \frac{\left(\frac{\bar{v}}{v_1} \right) [\ln(1-v_{2,s}) + v_{2,s} + \chi_1 v_{2,s}^2]}{v_{2,r} \left[\left(\frac{v_{2,s}}{v_{2,r}} \right)^{\frac{1}{3}} - \left(\frac{v_{2,s}}{v_{2,r}} \right) \right]} \quad (2)$$

where \overline{M}_n is the molecular weight of the uncrosslinked polymer, \bar{v} is the specific volume of the polymer, V_l is the molar volume of the solvent (18 cm³/mol for water), $v_{2,s}$ is the polymer volume fraction in the swollen hydrogel, $v_{2,r}$ is the polymer volume fraction in the hydrogel immediately upon crosslinking, and χ_l is the interaction parameter between the polymer and the solvent (0.426 for PEG in water). The mesh size was then determined³⁴ by first calculating the root mean square value from end-to-end of the polymer chain:

$$\sqrt{r_0^2} = lC_n^{1/2}n^{1/2} \quad (3)$$

where l is the average bond length (0.146 nm), C_n is the characteristic ratio of the PEG polymer (4.0), and n is the number of bonds present in the crosslink calculated by:

$$n = 2 \frac{\overline{M}_c}{M_r} \quad (4)$$

where M_r is the repeat unit molecular weight for the PEG polymer (44 g/mol for PEG). The mesh size was determined by the following equation:

$$\xi = v_2^{-1/3}(r_0^2)^{1/2} \quad (5)$$

2.7. Resistivity Measurements

To measure the resistivity of hydrogels, hydrogels were swollen in DI water for 24 hrs at room temperature and excess surface water was carefully removed with a KimWipe. The samples were then placed on a non-conductive surface, such as a petri dish, and 2 copper prongs (each 0.7 mm thick) spaced 8 mm apart were positioned directly in the hydrogel slab. The resulting resistance was recorded through an LCR meter (4284 A, 20 Hz – 1 MHz Precision meter, Hewlett Packard, Palo Alto, CA) with a frequency of 1 kHz and a voltage input of 1 V. The measured resistance was then converted into resistivity:

$$\rho = R \left(\frac{A}{L} \right) \quad (6)$$

where ρ is the resistivity of the hydrogel, R is the resistance measured, A is the cross-sectional area (0.7 mm thick prongs x 1 mm thick hydrogel), and L is the length between the prongs.

2.8. Cell Maintenance

The neural-like PC12 cells derived from a pheochromocytoma of the adrenal medulla in rats were used in this study. Cells were maintained under standard conditions in a RPMI medium containing 10% fetal bovine serum (FBS) and 1% penicillin/streptomycin in a humidified incubator at 37°C and 5% CO₂. Cells were passaged at 80% confluency (~ every 4-5 days) with change in media every 2 days. Only cells up to passage 20 were used for all experiments.

2.9. Cell Viability in 3D Composite Hydrogels

To test cell viability inside the 3D hydrogel scaffolds, hydrogels were prepared as described above with and without CNTs with two main differences. All hydrogels were prepared from sterile solutions and under sterile conditions. Cell suspension (1.8×10^6 cells/mL) in a complete medium (RPMI, 10% FBS, 1% pen/strep) was added directly to the hydrogel precursor solution at a 1:2 volumetric ratio. The cell-containing hydrogel precursor solution was gently mixed by pipetting up and down and 50 μ l aliquots were transferred onto the well bottom of a 24-well plate. The hydrogels were allowed to solidify in a humidified incubator at 37°C and 5% CO₂ for 20 min to achieve complete gelation. The gels were then soaked in a complete medium and left in the incubator for the remainder of the experiment. Cell viability was measured at 2 hrs, 24 hrs, and 72 hrs via live/dead staining. For live/dead staining, prior to encapsulation, PC12 cells were stained with 4 μ l/mL of 3,3'-diocetadecloxycarbocyanine perchlorate (DiOC₆, green membrane-

permeable dye) in a complete medium, incubated for 24 hrs before experimentation, and collected by a 5 min exposure to Trypsin/EDTA. Propidium Iodide (PI, red membrane-impermeable dye) at 2 $\mu\text{l}/\text{mL}$ was used to stain dead cells at the completion of the designated time points. Briefly, hydrogel-encapsulated cells were incubated with PI for 30 min, washed gently with fresh medium, and imaged under an inverted fluorescent microscope (Zeiss, Axiovert 200M, Oberkochen, Germany) at 10X zoom. The number of dead cells (red) and the total number of cells (green) were counted using the free ImageJ software (Cell Counter plugin) and percent cell viability was determined for each hydrogel condition as follows:

$$\% \text{ Cell Viability} = \left[1 - \left(\frac{\text{dead}}{\text{all}} \right) \right] \times 100\% \quad (7)$$

A minimum of three images were analyzed for each condition from at least three independent experiments.

2.10. Cryo-SEM Imaging

For cryo-scanning electron microscopy (SEM) imaging, all hydrogel samples were first flash frozen in liquid nitrogen. To flash freeze, tongs with metallic blocks on the tips were used to freeze the samples by submerging the prongs into a bath of liquid nitrogen. Once the temperature of the blocks was stabilized, a hydrogel sample was placed between the two blocks for 20 sec. The sample was lyophilized at -80°C and 15 mT for 24 hrs (VirTis Sentry 2.0, SP Scientific, Warminster, PA), sputter coated (SCD 005, Bal-Tec, Leica Microsystems, Buffalo Grove, IL) with gold and imaged via SEM (Zeiss EVO LS15 SEM, Oberkochen, Germany). Images were taken at a low voltage of 1.5 kV and a 500X magnification under a high vacuum environment.

2.11. Statistical Analysis

Results are reported as averages \pm standard deviation. Statistical significance between multiple samples was tested by ANOVA and between two samples by a student's t-test ($p < 0.05$) followed by a post-hoc analysis. A minimum of three samples from three independent experiments were tested per condition.

3. Results and Discussion

3.1. Dispersion of CNTs in Polymer Precursor Solution

The hydrophobicity and the high aspect ratio (~ 150) of the CNTs used in this study and hence high surface area, makes the individual CNTs susceptible to aggregation due to attractive Van der Waals forces, which in turn makes the dispersion of CNTs in an aqueous solution difficult.³⁵ Therefore, we investigated various methods of dispersion including mechanical disruption of the aggregates by sonication and chemical disruption by the use of surfactants. Note that linear unmodified PEG-diOH solution was used as opposed to 4-arm PEG acrylate in all dispersion studies to isolate the effect of the PEG polymer on CNT dispersion: previous studies have shown that PEG alone is an effective surfactant for CNTs within an aqueous solution.^{35, 36}

3.1.1. Dispersion of CNTs in Polymer Precursor Solution as a Function of Sonication Time

Several considerations were taken into account when investigating the effect of sonication on CNT dispersion. First, high intensity sonication (> 20 Hz) has been shown to fragment CNTs into smaller particles,^{35, 37, 38} thus, we chose a sonication method with medium power (6.75 Hz) to minimize CNT fragmentation. We chose a pulse sonication method where a pause between short sonication intervals was employed to prevent overheating and evaporation of the solution.^{39, 40}

Based on previous literature findings,^{18,40,41} we elected to use two conditions to disperse the CNTs: a long interval (20 seconds on/10 seconds off) and a short interval (1 second on/1 second off). Lastly, a total sonication time of 10 min including pauses was used to avoid possible CNT fragmentation, which has been shown to occur for continuous sonication times >5 min.⁴²

The effect of sonication time on CNT dispersion was studied for hydrogel precursor solutions containing PEG (10% w/v), CNTs (0.05% w/v), and BSA as an additional surfactant (0.05% w/v). A visual observation of phase contrast microscope images suggested that both sonication regimes were equally effective at CNT dispersion (Figure 1A). While qualitative analysis by means of identifying the appearance of the solution are a common practice,^{43,44} we also utilized a quantitative approach by analyzing the average area of aggregates as well as measuring the absorbance of the CNT/polymer solution. We observed larger CNT aggregates in the absence of sonication and significantly smaller aggregates with either mode of sonication (Figure 1B). Specifically, in the absence of sonication, the average area of aggregates was $1500 \mu\text{m}^2$ while sonicating with either condition resulted in an average aggregate area of $\sim 200 \mu\text{m}^2$ – an 87% decrease. Note that the targeted aggregate size was less than $350 \mu\text{m}^2$, a result which has been described as adequate dispersion in previous studies.³⁶ We also used absorbance - visible to infrared spectrum - to further determine the effect of a sonication regime on CNT dispersion, where higher absorbance values, i.e. more uniformly black solution, indicate a better dispersion.^{39,45} Figure 1C shows that the 20 sec on/10 sec off and 1 sec on/1 sec off sonication times had an equal absorbance rating that was 72% higher than the absorbance in the absence of sonication. In summary, we observed no significant difference in CNT dispersion between the 20 sec on/10 sec off and 1 sec on/1 sec off sonication time intervals; thus, we concluded that both

methods were equally effective for CNT dispersion under the conditions chosen for this study. We elected to use the 1 sec on/1 sec off sonication regime for all further experiments, unless otherwise noted.

3.1.2. Dispersion of CNTs in Polymer Precursor Solution as a Function of Surfactant

We also examined the effect of chemical disruption by surfactants of CNT aggregates within the PEG/CNT composite solution. Surfactants are commonly used to aid carbon nanotube dispersion in aqueous solutions³⁵ because they lower the surface tension of the carbon nanotubes, improving their wettability by the solution.^{36, 46} We specifically focused on surfactants, namely DMSO, BSA, sodium cholate, and laminin, which have been shown non-cytotoxic so that the developed composite hydrogel could be used for *in-situ* cell encapsulation. DMSO is an organic solvent which has been shown to dissociate CNT aggregates by coating the individual nanotubes and creating a stable suspension for up to 2 days.⁴⁷ BSA has been shown to disperse CNTs due to its electrostatic charge:^{48, 49} at a basic pH BSA becomes anionic and provides an electrostatic hindrance which causes a repulsion between the aggregates, effectively breaking the larger aggregates into smaller ones.⁴⁸⁻⁵⁰ Similarly, another anionic substance, namely sodium cholate, has also been shown very effective in dispersing CNTs within an aqueous solution.^{39, 45} Importantly, some studies report sodium cholate to be non-cytotoxic at concentrations below 1% w/v.⁷ Laminin was also chosen even though it has not been reported as a surfactant, because it promotes cell adhesion and proliferation and is especially beneficial for neural cell culture.^{51, 52} Furthermore, it has been shown that many proteins have the potential to promote CNT dispersion by adsorbing to the CNT surface by pi-pi stacking increasing the CNT hydrophilicity.⁵³ The sonication process in the presence of proteins has also been shown to aid dispersion by first

breaking the CNT aggregates and exposing them to the protein, and then by denaturing the protein itself and exposing its hydrophobic residues.⁵⁴ However, no direct correlation between protein properties (e.g. hydrophobicity, net charge) has yet been established.⁵⁴

The dispersion of CNTs as a function of additional surfactant is depicted in Figure 2. The absence of any additional surfactant (besides the PEG polymer itself) was used as a negative control. Samples with 1% sodium cholate and 0.05% BSA exhibited the best dispersion followed by laminin (Figure 2A), while addition of DMSO or 0.1% sodium cholate did not seem to have an added benefit over the PEG alone. Sodium cholate at 1% w/v dispersed the CNT aggregates into an average area of $\sim 35 \mu\text{m}^2$ and BSA into aggregates of $\sim 220 \mu\text{m}^2$, a significant decrease in average area with respect to no surfactant added ($\sim 1760 \mu\text{m}^2$), yielding a 98% and 87.5% change, respectively (Figure 2B). Dispersion with laminin also had a significant effect on the average CNT aggregate size: $\sim 970 \mu\text{m}^2$ - a 45% reduction as compared to PEG alone. No significant difference in CNT aggregate size was observed for the 1% DMSO or the 0.1% sodium cholate as compared to PEG alone. Absorbance measurements of the PEG/CNT/surfactant solutions confirmed the trends discussed above (Figure 2C). In the absence of a surfactant, we observed the absorbance for BSA and 1% sodium cholate to be very similar, ~ 2.7 - a 52% increase compared to the absorbance of PEG alone (~ 1.3). The increased absorbance values are in agreement with previous reports on CNT dispersion by means of BSA and sodium cholate.^{39, 55} The addition of 10% w/v laminin also yielded a higher absorbance of ~ 2.23 compared to no additional surfactant, albeit a lower absorbance than BSA or sodium cholate. DMSO and 0.1% sodium cholate were again shown ineffective at CNT dispersion.

In summary, in agreement with previous studies,^{39, 45, 55} we determined that both 0.05% BSA and 1% sodium cholate were efficient surfactants for CNT dispersion in an aqueous solution. While the 1% sodium cholate performed better than the BSA in terms of CNT dispersion, we chose BSA for all further experiments: in our study 1% w/v sodium cholate led to ~90% loss in PC12 cell viability at 2 hrs (Figure 1S).

3.2. Dispersion of CNTs in PEG Hydrogel

CNTs were added to the hydrogel precursor solution and then the solution was left to gel for up to 30 min. During that gelation time, there was a potential for CNT settling due to gravity^{39, 56} because of the higher CNT density ($\sim 2.1 \text{ g/cm}^3$)⁵⁷ as compared to a PEG aqueous solution ($\sim 1.2 \text{ g/cm}^3$).⁵⁸ To confirm even CNT dispersion, we examined CNT density as a function of hydrogel depth. Figure 3A shows a phase contrast image of a cross-section of the PEG-CNT hydrogel composite partitioned into 5 equivalent sections. We determined that there was a similar number of CNT aggregates within each section (~ 300) (Figure 3C), with a total area of $\sim 20 \times 10^3 \mu\text{m}^2$ (Figure 3D) and an average aggregate area of $\sim 70 \mu\text{m}^2$ (Figure 3B). Therefore, we concluded that the CNTs were evenly distributed throughout the hydrogel.

Interestingly, comparing the CNT aggregate size between the PEG-diOH solution and PEG-CNT hydrogel, we observed that the average aggregate size in the solution was $\sim 220 \mu\text{m}^2$ while the average aggregate size in the hydrogel was $\sim 70 \mu\text{m}^2$. To explain this difference we used each PEG constituent of the hydrogel (4-arm PEG-Ac and PEG-diSH) as a solution for the dispersion of CNTs (Figure 4). We determined that the 4-arm PEG-Ac solution was more effective in the dispersion of CNTs than the PEG-diOH solution, resulting in average aggregate size of $\sim 39 \mu\text{m}^2$

– an 82% change. There was no significant difference in CNT aggregate size between PEG-diOH and PEG-diSH solutions. Thus, the efficacy of the 4-arm PEG-Ac polymer in dispersing the CNTs can be explained by the substitution of the hydroxyl group of PEG-diOH with the hydrophobic acrylate group of the 4-arm PEG-Ac which contains an unsaturated carbon bond. Unsaturated carbon bonds have π -electronic affinity towards the CNT benzene rings.³⁶ Since the gel was prepared by sonicating the CNTs in the presence of 4-arm PEG-Ac, we concluded that the 4-arm PEG-Ac contributed to the smaller average aggregate size in the hydrogel.

3.3. Gelation Time

Figure 5 shows that gelation time increased for increasing concentrations of CNTs. For the lowest concentration of CNTs used in this study, namely 0.01% w/v, the gelation time was similar to that of the hydrogel without CNTs (~7.7 min). However, a slight but significant increase in gelation time was observed for 0.03% w/v CNTs (~7.8 min). This trend continued showing almost a linear increase in gelation time to ~13.8 min for 1.20% w/v CNTs - a 44% increase compared to the hydrogel without CNTs. Note that 1.20% w/v was used as the highest CNT concentration because the gel stopped forming at higher CNT concentrations. The CNT interference with the gelation kinetics was anticipated: Aktas et al. observed that the gelation time of polyacrylamide hydrogels was delayed at a threshold CNT concentration of 0.06% w/v while lower CNT concentrations had little to no effect on gelation.¹⁵ CNTs physically interfere with the crosslinking of the hydrogel resulting in a lower overall crosslink density and longer gelation times.¹⁸

3.4. Characterization of PEG-CNT Composite Hydrogels Mechanical Properties

The effect of the CNT presence and concentration on the viscoelastic properties of the hydrogel was investigated via rheology. We first performed an amplitude sweep (G' as a function of strain) on a hydrogel without CNTs in order to establish a strain value within the linear viscoelastic region (LVR). Previous studies have shown that small magnitudes of frequency are efficient in characterizing the stiffness of hydrogels in order to minimize oscillatory shear strain.^{27, 59, 60} Hence, G' measurements were conducted at a low constant strain (2%) as a function of frequency from 1 to 10 Hz. As anticipated for a viscoelastic crosslinked polymer, it was demonstrated that both storage modulus, G' , and loss modulus, G'' , were independent of frequency for low frequency (Figure 6A & 6B). Corroborating our results, it has been previously shown that the storage modulus of a UV-crosslinked PEG-dimethacrylate hydrogel was independent of frequency up to 100 Hz even when CNTs were added, as long as the CNTs were well dispersed within the hydrogel.³

We further observed that the stiffness of the PEG-CNT composite hydrogels changed as the concentration of CNTs increased from 0% w/v to 1.20% w/v (Figure 6C). Hydrogels without CNTs as well as low concentrations of CNTs up to 0.03% w/v exhibited higher moduli compared to gels with higher CNT concentrations. We observed a significant decrease in stiffness (37.5%) between the 0.03% w/v and 0.05% w/v CNT concentration. This result was unexpected as other studies have shown increase in hydrogel stiffness with addition of CNTs.¹⁸ Specifically, according to the rubber elasticity theory, the elastic modulus would increase with the addition of particulate solids (i.e. CNTs).⁶¹ However, the theory also states that the modulus of a material is directly proportional to the number of crosslinks.⁶¹ Thus, we suggest that due to the high aspect ratio of the CNTs, they could disrupt the crosslinking between the polymer and crosslinker,

resulting in a lower modulus - a phenomena also demonstrated by others.⁶⁰ The high aspect ratio of the CNTs also means that they have a large surface area and, thus, a large interfacial region between the CNTs and the polymer molecules, leading to decreased mobility of the polymer chains in the vicinity of the CNTs.⁶² Such decreased polymer mobility in the vicinity of CNTs has been shown to result in a lower crosslinking density and consequently a lower storage modulus.³ Therefore, we suggest that competing effects of strengthening the hydrogel modulus by the addition of stiffer particulates (stiffness of individual CNT is ~ 1 TPa)⁶³ and compromising the crosslinking efficiency could explain the decrease in composite hydrogel modulus at a threshold CNT concentration of 0.03% w/v. However, the lower modulus with CNT addition could be beneficial for neural tissue engineering applications to reduce the stiffness mismatch with the soft neural tissue.

3.5. Characterization of PEG-CNT Composite Hydrogels Swelling and Mesh Size

In addition to the decrease in stiffness, lower crosslinking efficiency has also been shown to lead to an increase in swelling and mesh size of hydrogels.²¹ Thus, we further investigated the effect of CNT addition and concentration on these properties (Figure 7). Similarly to the storage modulus, we observed an abrupt and significant increase of 14% in Q_M when the CNT concentration was increased from 0.03% to 0.05% w/v. The same kind of change was observed in the hydrogel mesh size. A further increase in CNT concentration, up to 1.20% w/v, did not lead to a significant change in swelling ratio or mesh size. In comparing the rate of hydrogels' swelling (Figure 2S), we observed that the presence of CNTs did not affect the rate but only the equilibrium swelling of the hydrogels. Equilibrium in the absence of CNTs or at 0.05% w/v CNTs (the threshold value for which a significant change in Q_M was noted) was reached at ~ 2 h.

When comparing the storage modulus to the swelling behavior of the PEG-CNT composite hydrogels, we observed an inverse trend that has been shown in previous studies.³ Our results are comparable to previous studies incorporating CNTs into hydrogels^{3, 64, 65} and can be explained by decrease in crosslinking density.⁶¹ Lastly, we note that the resultant PEG-CNT hydrogel composites are nanoporous with mesh sizes in the order of ~13-16 nm based on the concentration of CNTs added.

To further understand the structural changes imposed by the CNTs, we imaged hydrogels without CNTs and with 0.20% w/v CNT-loaded hydrogels under SEM (Figure 8). A freeze drying method was used to generate a honeycomb structure and observe changes in gel structure with CNT addition. We observed a lower number of pores and larger pore size within the PEG-CNT composite than the hydrogel without CNTs, albeit in the micron-size. According to the mesh size calculated earlier, we expected that the pore size of the hydrogel samples would be in the nanomolar range. However, we would like to emphasize that the mesh size calculated earlier is based on a theory that does not take into account the CNT properties. This discrepancy between theory and SEM images could also be partially explained by the flash-freezing in DI water which could have caused these micron-sized porous structures by mechanical disruption of the hydrogel. Decrease or increase in overall hydrogel porosity with addition of CNTs has been noted by many and has been linked to the specific hydrogel parameters and interaction with the CNTs.^{19, 66} Specifically for our hydrogel system, we suggest that the overall decrease in the number of pores was related to the hydrophobic nature of the CNTs and their ability to displace hydrophilic components and thus decrease the density of the hydrophilic hydrogel network.⁶⁶ The larger pore size on the other hand could be related to the overall increase in swelling.

3.6. Characterization of PEG-CNT Composite Hydrogel Electrical Conductivity

We observed a decrease in resistivity with increasing concentrations of CNTs (Figure 9). The resistivity of the hydrogels without CNTs was $0.88 \Omega\text{m}$ and the resistivity significantly decreased to $0.76 \Omega\text{m}$ with the inclusion of CNTs even at 0.01% w/v (a change of $\sim 13\%$). The resistivity decreased further down to $0.50 \Omega\text{m}$ for the highest CNT concentration studied for a total decrease of 43% . This result was expected as previous studies have reported an increase in conductivity (decrease in resistivity) due to capacitive currents and the formation of a conductive pathway with the addition of dispersed CNTs.²⁰ Furthermore, in comparing resistivity to hydrogel swelling, we note that at lower CNT loading ($<0.05\%$ w/v), increase in hydrogel swelling could also be contributing to decrease in resistivity: a slight but significant decrease in resistivity can also be achieved by decreasing the polymer precursor concentration and hence the hydrogel swelling (data not shown). However, we note that at higher CNT loading ($\geq 0.05\%$ w/v), trends in resistivity no longer correlate with hydrogel swelling.

We further noted that the resistivity is closely related to the level of dispersion of the CNTs: resistivity of the hydrogels was lower for better dispersed CNTs (Figure 3S). The effect of CNT dispersion, hence percolation, on CNT-hydrogel composites has been previously noted.²⁰ Electrical percolation occurs when long, continuous pathways are created within the hydrogel. For CNT-hydrogel composites, the continuity of the conductive pathways is directly proportional to the CNT loading and alignment: the higher the loading or the better the alignment, the higher the conductivity should be. For the hydrogels developed here, both loading and dispersion improved conductivity but we were not able to pass the percolation threshold. Hallmarks of electrical percolation in composite materials are the sudden increase in electrical conductivity

and the retaining of optical clarity of the sample:⁶⁷ we did not observe a sudden decrease in resistivity (Figure 9) and the addition of CNTs generally decreased the optical clarity of the hydrogels (Figure 4S). However, we demonstrated that the inclusion of CNTs even at a very low CNT loading of 0.01% w/v led to a significant decrease in composite hydrogel resistivity.

3.7. Effect of PEG-CNT Composite Hydrogels on Cell Viability

We examined the effect of CNTs and CNT-surfactant combinations on PC12 cell viability. PC12 cells are a neural-like cell line and a well-accepted model to study nerve regeneration due to their inducible differentiation to a neuronal phenotype.²⁴ We did not anticipate that the hydrogel itself or the presence of CNTs would have an adverse effect on the cells: PEG has been previously shown compatible with PC12 cells encapsulation²⁴ and CNTs, in the concentration range used in this study, embedded in a hydrogel matrix or attached to a surface have been determined non-cytotoxic to cells.^{12, 18, 68} Here we used an unmodified PEG hydrogel where the CNTs or the CNT-surfactant combination and not the PEG could present attachment sites for the PC12 cells. Figure 10 shows the PC12 cell viability as a function of CNT-surfactant combinations at 2 hrs – to determine if the hydrogel encapsulation alone affected cell viability, and 72 hrs – to determine the extent of cell adaptation to the hydrogel scaffold. Representative fluorescent images of the performed live/dead assay on the cells encapsulated in the composite hydrogels are presented in Figure 5S, where all cells were stained green and dead cell nuclei were stained red (image inserts). Specifically, we examined the following conditions: tissue culture plastic (TCP) as a positive control, hydrogel with no added CNTs (Pristine), gel with 0.05% w/v CNTs but no surfactant (+CNTs), gel with 0.05% w/v CNTs and 0.05% w/v BSA as a surfactant

(+CNTs/+BSA), and gel with 0.05% w/v CNTs, as well as 0.05% w/v BSA and 100 $\mu\text{g/ml}$ laminin as surfactants (+CNTs/+BSA/+LAM).

Note that unlike the TCP positive control, all other live/dead studies were conducted for a 3D cell culture, i.e. cells encapsulated in the composite hydrogels. Thus, even though care was taken not to dislodge the dead cells on the TCP prior to cell imaging, i.e. no washes were performed on the cells after staining and prior to imaging, it is possible that not all dead cells on the TCP were accounted for. In part, this could explain the slightly higher cell viability on TCP as compared to all other 3D conditions. When comparing all 3D conditions, the greatest decrease in cell viability occurred in the hydrogels without CNTs: at 2 hrs the viability was $\sim 84\%$, decreasing by $\sim 50\%$ at 72 hrs. The initially high cell viability at 2 hrs, which was comparable to the rest of the 3D encapsulation conditions, indicated that the encapsulation conditions alone did not contribute to the overall lower cell viability. Instead, the decrease in cell viability was attributed to the lack of attachment sites on the PEG hydrogel and the resulting inability of the hydrogel to support long term culture of attachment-dependent cells. Such attachment-dependent PC12 cell viability in similar PEG hydrogels has been reported previously.²⁴ Once the CNTs were dispersed in the absence of additional surfactants, the 2 hrs cell viability was high, $\sim 87\%$, with a slight but significant decrease of $\sim 11\%$ at 72 hrs. The higher 72 hr cell viability as compared to the hydrogel without CNTs indicated that the CNTs provided attachment sites for the PC12 cells, a phenomenon reported by others as well.^{18, 19, 69}

We then analyzed the effect of 0.05% BSA on cell viability and observed a similar trend compared to the condition without BSA: 84% viability at 2 hrs and 77% viability at 72 hrs or

~7% total decrease in viability over the chosen time interval. BSA has been shown to effectively block cell adhesion by occupying non-specific sites of attachment,⁷⁰ thus, we did not expect improvement in cell viability over the CNT only condition. However, the fact that we also did not observe lower cell viability than the CNT only condition indicated that not all CNT surface area was occupied by the BSA molecules and consequently cell attachment was not completely inhibited. To improve cell viability at 72 h, we used laminin, an extracellular matrix protein that effectively promotes integrin binding,⁵² in addition to the BSA. As anticipated, in the presence of laminin and BSA, the cell viability at 2 hrs was measured to be ~89% and had a minimal decrease of 4.5% over 72 hrs. Lastly, to confirm that cell viability in the PEG hydrogel was indeed related to cell attachment, we seeded cells on top of the PEG-CNT hydrogel composites (Figure 6S). As anticipated, we observed that cells did not attach to the PEG hydrogel in the absence of CNTs, but could attach to the CNT-PEG hydrogels. Similarly to the 3D encapsulation, the highest cell viability for the 2D condition was observed for the laminin-BSA and laminin only coated composite hydrogels. Notably, when cells were seeded on the surface of a laminin coated PEG-CNT hydrogel, the cells preferentially clustered around the CNTs and extended processes between CNT aggregates (Figure 6S), indicating that the CNTs were acting as anchorage sites for the cells possibly due to their excellent ability to adsorb proteins.⁵⁴

4. Conclusions

In this study, CNTs were successfully dispersed within a PEG hydrogel by optimizing sonication times and surfactants. The resultant hydrogel-CNT composite was then thoroughly characterized. We determined that an increase in CNT concentration resulted in increased gelation time, decreased hydrogel stiffness after a threshold CNT concentration of 0.03% w/v with a

corresponding increase in swelling and mesh size, and a decrease in composite hydrogel resistivity. The hydrogel was also found compatible with PC12 cell culture supporting higher cell viability in the presence of CNTs than in the PEG hydrogel alone. Biocompatible and electroconductive PEG-CNT composite hydrogels, as the ones developed here, have potential uses in the fields of neural tissue engineering, sensor technology as electrode coatings, and drug delivery.

5. Acknowledgements

We would like to acknowledge support from start-up funds provided to Dr. Zustiak by Saint Louis University as well as a Graduate Assistantship awarded to Keval Shah by Saint Louis University. We also thank Dr. Irma Kuljanishvilli for helpful discussions regarding CNTs and Dr. Kyle Mitchell for the use of his RLC meter.

FIGURE CAPTIONS:

Figure 1. Dispersion of CNTs as a function of sonication time. A 0.05% w/v CNT concentration and 0.05% BSA surfactant were added to a 10% PEG-diOH polymer solution and sonicated for different times: no sonication, 20 sec on/10 sec off, 1 sec on/1 sec off. Images of the resulting solutions were taken under a light microscope (scale bar = 200 μm) **(A)** and analyzed via Image J, to determine the average particle area (significant differences in comparison to no-sonication control are designated by an asterisk for $n = 6$; $p < 0.05$) **(B)**. Average solution absorbance was measured via spectrophotometry ($n = 3$; $p < 0.05$) **(C)**.

Figure 2. Dispersion of CNTs as a function of surfactant. CNTs at a concentration of 0.05% w/v were added to a 10% PEG-diOH polymer solution and sonicated at a constant 1 on/1 off sonication time with different surfactants: No surfactant, 0.05% BSA, 10% Laminin, 1% DMSO, 0.10% Sodium Cholate, and 1% Sodium Cholate. Images of the resulting solutions were taken under a light microscope (scale bar = 200 μm) **(A)** and analyzed via Image J, to determine the average particle area (significant differences in comparison to no surfactant control are designated by an asterisk for $n = 6$; $p < 0.05$) **(B)**. Average solution absorbance was measured via spectrophotometry ($n = 3$; $p < 0.05$) **(C)**.

Figure 3. CNT distribution within PEG-CNT hydrogel composite as a function of hydrogel depth. Phase contrast image of the distribution of CNTs within a 1 mm thick hydrogel sectioned into 200 μm wide sections **(A)**. The sections were then analyzed for number of CNT aggregates per section **(B)**, an average area of CNT aggregates per section **(C)**, and a total area of CNT aggregates per section **(D)**. No significant difference between sections was noted ($n = 3$; $p < 0.05$).

Figure 4. Dispersion of CNTs as a function of PEG constituents. CNTs at a concentration of 0.05% w/v were added to a 10% PEG-diOH, 10% 4-arm PEG-Ac, 10% PEG-diSH polymer solution and sonicated at a constant 1 on/1 off sonication time with 0.05% w/v BSA surfactant. Images of the resulting solutions were taken under a light microscope (scale bar = 200 μm) (A) and analyzed via Image J, to determine the average particle area (significant differences in comparison to PEG-diOH condition are designated by an asterisk for $n = 3$; $p < 0.05$) (B).

Figure 5. Gelation time of PEG-CNT composite hydrogel increases with increase in CNT concentration. Significant differences are denoted by asterisks ($n = 3$, $p < 0.05$).

Figure 6. Mechanical characterization of PEG-CNT composite hydrogels. Hydrogel samples were tested via rheological analysis to measure their respective storage modulus (G') and loss modulus (G'') as a function of CNT concentration. An example of rheology data is shown for hydrogels without CNTs (0.00% w/v) (A) and 0.20% w/v CNTs (B). Storage modulus as a function of CNT concentration (C). Significant differences as compared to the hydrogels without CNTs are designated by asterisk ($n = 4$, $p < 0.05$).

Figure 7. Swelling behavior of PEG-CNT composite hydrogels. The swelling ratio (Q_M) and the corresponding mesh size (ζ) of hydrogels as a function of CNT concentration. Significant differences as compared to the hydrogel without CNTs (0.00% w/v) for Q_M and ζ are designated by an asterisk and plus sign, respectively ($n = 4$, $p < 0.05$).

Figure 8. Pore size analysis of hydrogels. Qualitative depiction of the pore size difference between a PEG hydrogel without CNTs (**A**) and 0.2% PEG-CNT composite hydrogel (**B**). Images taken at 500x magnification.

Figure 9. Resistivity characterization of PEG-CNT composite hydrogels. Resistivity measurements showed a significant decrease from 0.00% w/v to 0.10% w/v CNTs along with the remaining concentrations of CNTs. Significant differences as compared to the hydrogel without CNTs (0.00% w/v) are designated by an asterisk ($n = 3, p < 0.05$). Once 0.20% w/v CNTs were dispersed, the BSA concentration was increased in proportion to the CNT concentration.

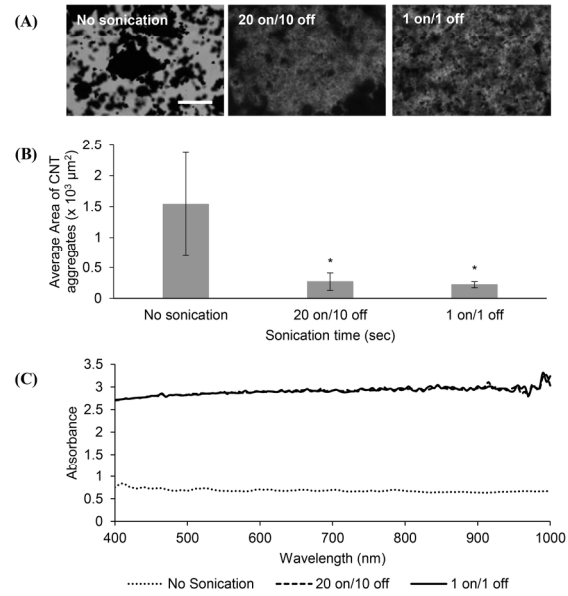
Figure 10. PC12 cell viability within PEG-CNT composite hydrogels as a function of time. PC12 cells were encapsulated within the various hydrogel samples and stained with DiOC (green) and PI (red) for fluorescence microscopy analysis. Using ImageJ software, the percent cell viability as a function of time was determined for the various CNT/surfactant combinations studied. Significant differences between respective time points for each condition are designated by an asterisk. Significant differences compared to hydrogel without CNTs or surfactants (Pristine), +CNTs, and +CNTs/+BSA for each time point are designated by +, ++, and +++, respectively ($n = 3; p < 0.05$).

References:

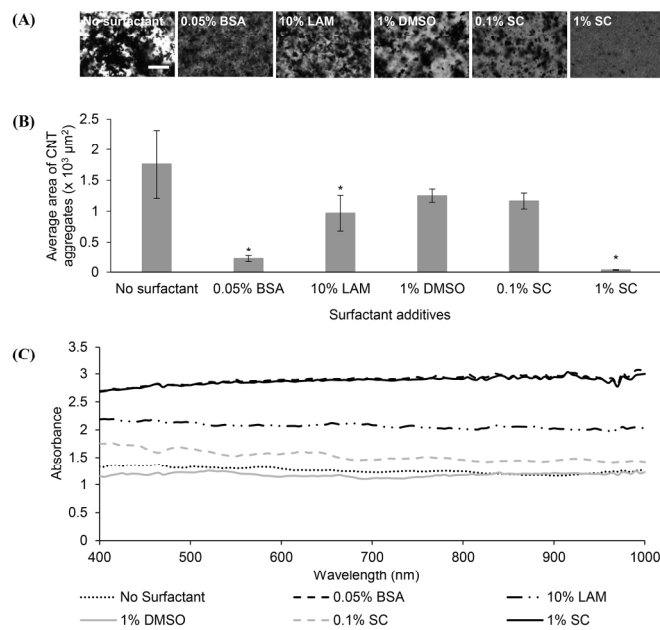
1. A. S. Hoffman, *Advanced drug delivery reviews*, 2012, **64**, 18-23.
2. C. Journet, M. Picher and V. Jourdain, *Nanotechnology*, 2012, **23**, 142001.
3. S. Vural, K. B. Dikovics and D. M. Kalyon, *Soft Matter*, 2010, **6**, 3870.
4. M. Foldvari and M. Bagonluri, *Nanomedicine: Nanotechnology, Biology and Medicine*, 2008, **4**, 173-182.
5. L. Belyanskaya, S. Weigel, C. Hirsch, U. Tobler, H. F. Krug and P. Wick, *Neurotoxicology*, 2009, **30**, 702-711.
6. Y. Cho and R. B. Borgens, *Journal of biomedical materials research. Part A*, 2010, **95**, 510-517.
7. L. Dong, K. L. Joseph, C. M. Witkowski and M. M. Craig, *Nanotechnology*, 2008, **19**, 255702.
8. G. Cirillo, S. Hampel, U. G. Spizzirri, O. I. Parisi, N. Picci and F. Iemma, *BioMed research international*, 2014, **2014**.
9. M. C. Serrano, M. C. Gutiérrez and F. del Monte, *Progress in Polymer Science*, 2014, **39**, 1448-1471.
10. E. L. Hopley, S. Salmasi, D. M. Kalaskar and A. M. Seifalian, *Biotechnology advances*, 2014, **32**, 1000-1014.
11. C. M. Voge and J. P. Stegemann, *Journal of neural engineering*, 2011, **8**, 011001.
12. L. Ghasemi-Mobarakeh, M. P. Prabhakaran, M. Morshed, M. H. Nasr-Esfahani, H. Baharvand, S. Kiani, S. S. Al-Deyab and S. Ramakrishna, *Journal of tissue engineering and regenerative medicine*, 2011, **5**, e17-e35.
13. L. He, D. Lin, Y. Wang, Y. Xiao and J. Che, *Colloids and Surfaces B: Biointerfaces*, 2011, **87**, 273-279.
14. A. Fabbro, M. Prato and L. Ballerini, *Advanced drug delivery reviews*, 2013, **65**, 2034-2044.
15. D. K. Aktaş, G. A. Evingür and Ö. Pekcan, *Composite Interfaces*, 2010, **17**, 301-318.
16. T. I. Chao, S. Xiang, J. F. Lipstate, C. Wang and J. Lu, *Advanced Materials*, 2010, **22**, 3542-3547.
17. L. Y. Yan, H. Chen, P. Li, D.-H. Kim and M. B. Chan-Park, *ACS applied materials & interfaces*, 2012, **4**, 4610-4615.
18. S. R. Shin, H. Bae, J. M. Cha, J. Y. Mun, Y. C. Chen, H. Tekin, H. Shin, S. Farshchi, M. R. Dokmeci, S. Tang and A. Khademhosseini, *ACS nano*, 2012, **6**, 362-372.
19. S. R. Shin, S. M. Jung, M. Zalabany, K. Kim, P. Zorlutuna, S. b. Kim, M. Nikkhah, M. Khabiry, M. Azize and J. Kong, *ACS nano*, 2013, **7**, 2369-2380.
20. R. A. MacDonald, C. M. Voge, M. Kariolis and J. P. Stegemann, *Acta biomaterialia*, 2008, **4**, 1583-1592.
21. S. P. Zustiak and J. B. Leach, *Biomacromolecules*, 2010, **11**, 1348-1357.
22. P. Naghdi, T. Tiraihi, F. Ganji, S. Darabi, T. Taheri and H. Kazemi, *Journal of tissue engineering and regenerative medicine*, 2014.
23. R. Mooney, S. Haeger, R. Lawal, M. Mason, N. Shrestha, A. Laperle, K. Bjugstad and M. Mahoney, *Tissue Engineering Part A*, 2011, **17**, 2805-2815.
24. S. P. Zustiak, S. Pubill, A. Ribeiro and J. B. Leach, *Biotechnology progress*, 2013, **29**, 1255-1264.
25. Y. Xiao, L. He and J. Che, *Journal of Materials Chemistry*, 2012, **22**, 8076-8082.

26. J. A. Roman, T. L. Niedzielko, R. C. Haddon, V. Parpura and C. L. Floyd, *Journal of neurotrauma*, 2011, **28**, 2349-2362.
27. M. Lutolf and J. Hubbell, *Biomacromolecules*, 2003, **4**, 713-722.
28. C. A. Durst, M. P. Cuchiara, E. G. Mansfield, J. L. West and K. J. Grande-Allen, *Acta biomaterialia*, 2011, **7**, 2467-2476.
29. I. Mironi-Harpaz, D. Y. Wang, S. Venkatraman and D. Seliktar, *Acta biomaterialia*, 2012, **8**, 1838-1848.
30. C. G. Williams, A. N. Malik, T. K. Kim, P. N. Manson and J. H. Elisseeff, *Biomaterials*, 2005, **26**, 1211-1218.
31. J. L. Vanderhooft, B. K. Mann and G. D. Prestwich, *Biomacromolecules*, 2007, **8**, 2883-2889.
32. J. Baier Leach, K. A. Bivens, C. W. Patrick, Jr. and C. E. Schmidt, *Biotechnology and bioengineering*, 2003, **82**, 578-589.
33. N. A. Peppas, J. Z. Hilt, A. Khademhosseini and R. Langer, *ADVANCED MATERIALS-DEERFIELD BEACH THEN WEINHEIM-*, 2006, **18**, 1345.
34. T. Canal and N. A. Peppas, *Journal of Biomedical Materials Research*, 1989, **23**, 1183-1193.
35. L. Vaisman, H. D. Wagner and G. Marom, *Advances in colloid and interface science*, 2006, **128-130**, 37-46.
36. L. Vaisman, G. Marom and H. D. Wagner, *Advanced Functional Materials*, 2006, **16**, 357-363.
37. G. Gkikas, N.-M. Barkoula and A. Paipetis, *Composites Part B: Engineering*, 2012, **43**, 2697-2705.
38. M. D. Rossell, C. Kuebel, G. Ilari, F. Rechberger, F. J. Heiligtag, M. Niederberger, D. Koziej and R. Erni, *Carbon*, 2013, **61**, 404-411.
39. A. J. Blanch, C. E. Lenehan and J. S. Quinton, *The journal of physical chemistry. B*, 2010, **114**, 9805-9811.
40. M. Salam, M. Hosur, S. Zainuddin and S. Jeelani, *Open Journal of Composite Materials*, 2013, **3**, 1.
41. I. Yoon, K. Hamaguchi, I. V. Borzenets, G. Finkelstein, R. Mooney and B. R. Donald, *PloS one*, 2013, **8**, e65715.
42. K. Lu, R. Lago, Y. Chen, M. Green, P. Harris and S. Tsang, *Carbon*, 1996, **34**, 814-816.
43. R. Bandyopadhyaya, E. Nativ-Roth, O. Regev and R. Yerushalmi-Rozen, *Nano Letters*, 2002, **2**, 25-28.
44. X. Xin, G. Xu and H. Li, *Dispersion and Property Manipulation of Carbon Nanotubes by Self-Assemblies of Amphiphilic Molecules*, INTECH Open Access Publisher, 2013.
45. S. Lin and D. Blankschtein, *The journal of physical chemistry. B*, 2010, **114**, 15616-15625.
46. M. Shim, N. W. Shi Kam, R. J. Chen, Y. Li and H. Dai, *Nano Letters*, 2002, **2**, 285-288.
47. H. T. Ham, Y. S. Choi and I. J. Chung, *Journal of Colloid and Interface Science*, 2005, **286**, 216-223.
48. Z. Ji, X. Jin, S. George, T. Xia, H. Meng, X. Wang, E. Suarez, H. Zhang, E. M. Hoek and H. Godwin, *Environmental science & technology*, 2010, **44**, 7309-7314.
49. X. Wang, T. Xia, S. A. Ntim, Z. Ji, S. George, H. Meng, H. Zhang, V. Castranova, S. Mitra and A. E. Nel, *ACS nano*, 2010, **4**, 7241-7252.
50. E. Edri and O. Regev, *Analytical chemistry*, 2008, **80**, 4049-4054.

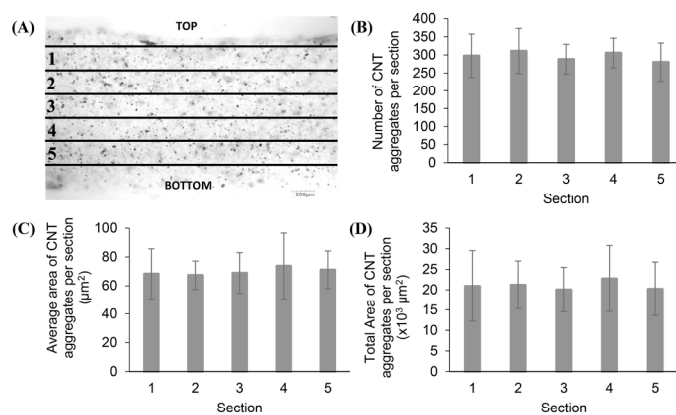
51. A. M. Baur, T. I. Gamberger, H. G. Weerda, M. Gjuric and E. R. Tamm, *Acta otolaryngologica*, 1995, **115**, 517-521.
52. K. J. Tomaselli, C. H. Damsky and L. F. Reichardt, *The Journal of cell biology*, 1987, **105**, 2347-2358.
53. R. Rastogi, R. Kaushal, S. Tripathi, A. L. Sharma, I. Kaur and L. M. Bharadwaj, *Journal of colloid and interface science*, 2008, **328**, 421-428.
54. K. Matsuura, T. Saito, T. Okazaki, S. Ohshima, M. Yumura and S. Iijima, *Chemical physics letters*, 2006, **429**, 497-502.
55. J. S. Kim, K. S. Song, J. H. Lee and I. J. Yu, *Archives of toxicology*, 2011, **85**, 1499-1508.
56. Y. Huang, Y. Zheng, W. Song, Y. Ma, J. Wu and L. Fan, *Composites Part A: Applied Science and Manufacturing*, 2011, **42**, 1398-1405.
57. Q. Lu, G. Keskar, R. Ciocan, R. Rao, R. B. Mathur, A. M. Rao and L. L. Larcom, *The Journal of Physical Chemistry B*, 2006, **110**, 24371-24376.
58. A. Eliassi, H. Modarress and G. A. Mansoori, *Journal of Chemical & Engineering Data*, 1998, **43**, 719-721.
59. M. J. Moura, M. M. Figueiredo and M. H. Gil, *Biomacromolecules*, 2007, **8**, 3823-3829.
60. S. Sathaye, A. Mbi, C. Sonmez, Y. Chen, D. L. Blair, J. P. Schneider and D. J. Pochan, *Wiley Interdisciplinary Reviews: Nanomedicine and Nanobiotechnology*, 2015, **7**, 34-68.
61. P. J. Flory, *Principles of polymer chemistry*, Cornell University Press, Ithaca,, 1953.
62. T. Ramanathan, H. Liu and L. Brinson, *Journal of Polymer Science Part B: Polymer Physics*, 2005, **43**, 2269-2279.
63. E. T. Thostenson, Z. Ren and T.-W. Chou, *Composites science and technology*, 2001, **61**, 1899-1912.
64. X. Tong, J. Zheng, Y. Lu, Z. Zhang and H. Cheng, *Materials Letters*, 2007, **61**, 1704-1706.
65. M. Xu, T. Zhang, B. Gu, J. Wu and Q. Chen, *Macromolecules*, 2006, **39**, 3540-3545.
66. Y.-S. Chen, P.-C. Tsou, J.-M. Lo, H.-C. Tsai, Y.-Z. Wang and G.-H. Hsiue, *Biomaterials*, 2013, **34**, 7328-7334.
67. E. Bilotti, H. Zhang, H. Deng, R. Zhang, Q. Fu and T. Peijs, *Composites Science and Technology*, 2013, **74**, 85-90.
68. S. R. Shin, H. Bae, J. M. Cha, J. Y. Mun, Y.-C. Chen, H. Tekin, H. Shin, S. Farshchi, M. R. Dokmeci and S. Tang, *ACS nano*, 2011, **6**, 362-372.
69. B. L. Behan, D. G. DeWitt, D. R. Bogdanowicz, A. N. Koppes, S. S. Bale and D. M. Thompson, *Journal of biomedical materials research. Part A*, 2011, **96**, 46-57.
70. X. Liu, L. Chen, H. Liu, G. Yang, P. Zhang, D. Han, S. Wang and L. Jiang, *NPG Asia Materials*, 2013, **5**, e63.



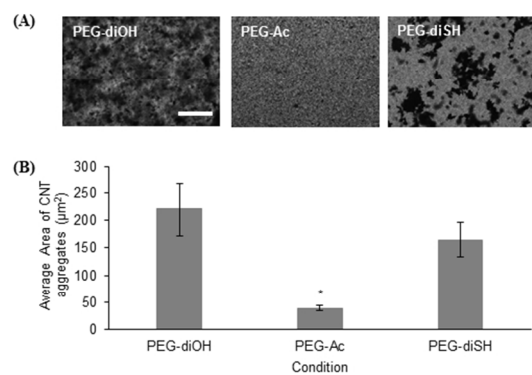
190x142mm (300 x 300 DPI)



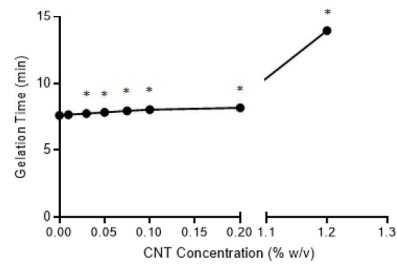
190x142mm (300 x 300 DPI)



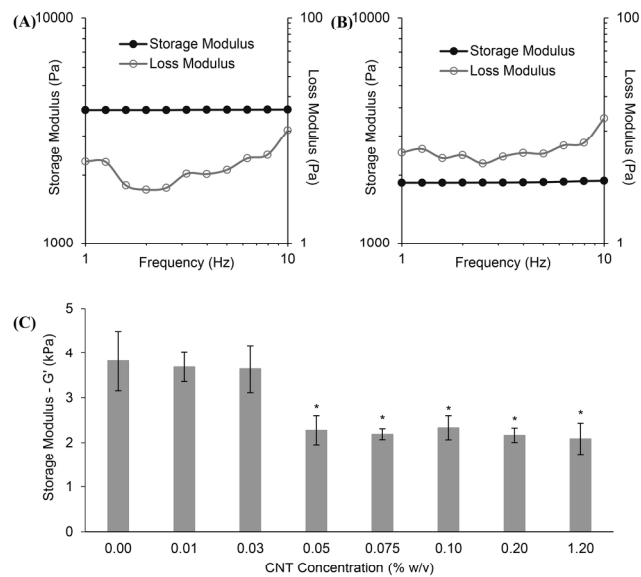
190x142mm (300 x 300 DPI)



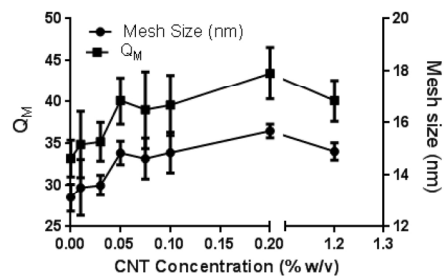
254x190mm (96 x 96 DPI)



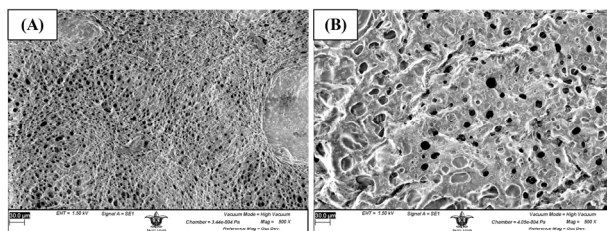
190x142mm (300 x 300 DPI)



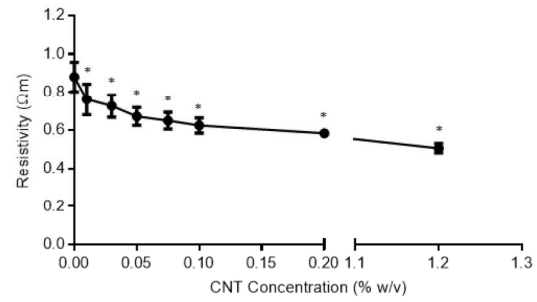
190x142mm (300 x 300 DPI)



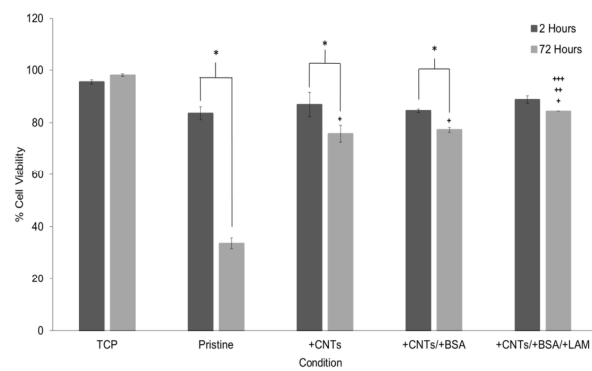
190x142mm (300 x 300 DPI)



190x142mm (300 x 300 DPI)



190x142mm (300 x 300 DPI)



190x142mm (300 x 300 DPI)